Acta Cryst. (1994). A**50**, 107–115

Bloch-Wave Degeneracies and Nonsystematic Critical Voltage: a Method for Structure-Factor Determination

BY H. MATSUHATA* AND J. GJØNNES

Department of Physics, University of Oslo, PO Box 1048 *Blindern*, 0316 *Oslo, Norway*

(*Received* 29 *March* 1993; *accepted* 12 *July* 1993)

Abstract

The critical-voltage method in electron diffraction is extended to nonsystematic cases. Precise determination of relations between structure factors can then be carried out in the usual voltage range for transmission electron microscopes. General analytical expressions for three- and four-beam cases are derived. High precision (0.1%) in the determination of structure factors (Fourier potential) is obtained in special symmetric cases. Theoretical analysis and experimental patterns are shown for three such examples: a four-beam case in diamond and sphalerite structures (silicon, ZnS), a five-beam case in a face-centred-cubic metal (copper) and a six-beam case in rock salt MgO. Several other cases are described and the effect of absorption is shown to be small.

1. Introduction

The critical-voltage effect in high-energy electron diffraction (Watanabe, Uyeda & Fukuhara, 1969) offers a sensitive method for structure-factor determination. Low-order structure factors can, in special cases, be determined with a precision better than 0.1% from the extinction of Kikuchi- or Kossel-line contrast at a particular voltage (Sellar, Imeson & Humphreys, 1980; Tabbernor, Fox & Fisher, 1990). Until recently, such measurements have been based almost exclusively on the systematic case, *viz* the extinction of a second-order line $2g$ owing to the interaction with the first-order reflection g. Apart from the need for high accelerating voltage, this systematic critical voltage was limited to the determination of one or two structure factors from very simple structures. Therefore, Gjønnes & Høier (1971) proposed to extend the method to nonsystematic cases. The application of critical voltages occurring at zone-axis positions was discussed by Shannon & Steeds (1977) (see also Matsuhata & Steeds, 1987), but so far no extensive discussion of the nonsystematic critical-voltage effect has been presented.

A basis for this discussion may be the treatment of dynamical scattering in the three-beam case, as presented by Gjønnes & Høier (1971) and Hurley & Moodie (1980); see also Kambe (1957). Any nonsystematic three-beam case 0, g, h in a centrosymmetric crystal will include Bloch-wave degeneracy at a particular set of excitation errors, visible as vanishing contrast at a certain position on the Kikuchi or Kossel line. Measurement of this condition, which can be carried out at normal voltages, might in principal yield two experimentally determined relations between structure factors. But in practice this condition will, in most cases, be difficult to measure with sufficient accuracy: special configurations must be sought in order to attain accuracies comparable with the systematic critical-voltage method.

The purpose of the present study has been to investigate such conditions theoretically and experimentally. The analytical treatment is extended to four beams and the role of symmetry in describing the effect is emphasized. The influence of absorption is discussed. Three typical situations are analysed in some detail: a diamond-shaped four-beam case, with 422, 220, 202 in face-centred-cubic (f.c.c.) structures (silicon, ZnS); extinction of a segment at the 420, 240 intersection consituting a five-beam case in a f.c.c. metal (copper); contrast anomaly in a six-beam case in an NaCl-type structure (MgO) involving the weak 111 reflection. The early measurements of critical effects were based on Kikuchi-line contrast. The sensitivity is increased when the corresponding Kossel-line features appearing in convergent-beam electron diffraction (CBED) discs are used instead (Sellar, Imeson & Humphreys, 1980). The continuously variable voltage available in modern electron microscopes operating in the range up to some hundred kV facilitates the measurement.

The contrast features observed correspond to Bloch-wave degeneracies and the Bloch-wave representation is a convenient basis for our discussion. The cases presented in this paper can be referred to a zero-order zone, with the usual simplifications associated with the transmission case, see *e.g.* Reimer (1989). Corrections pertinent to an inclined entrance surface can be applied, see *e.g.* Niehrs & Wagner

* Present address: Division of Electrodevices, Electrotechnical Laboratory, 1-1-4 Umezono, Tsukuba, Japan.

(1955), but are usually negligible. The disperson surface is represented by the *Anpassung* measured along the z direction as a function of the components k_x and k_y of the incident wave vector $\mathbf{k}$. Inversion symmetry in the zone is assumed and the symmetry of Bloch waves can then be described by the notation used by Cochran (1952). For a discussion of Bloch-wave symmetry, see Gjønnes & Taftø (1978) and Kogiso & Takahashi (1977).

2. Bloch-wave degeneracy in three- and four-beam cases

Let us first recall briefly the condition for degeneracy in the centrosymmetric three-beam case as studied by Gjønnes & Høier (1971), Gevers, Serneels & David (1974) and Hurley & Moodie (1980). The eigenvalue equation obtained from the three-beam dispersion matrix,

$$\begin{bmatrix} -2k\gamma & U_{12} & U_{13} \\ U_{11} & 2k(s_2-\gamma) & U_{23} \\ U_{31} & U_{23} & 2k(s_3-\gamma) \end{bmatrix},$$

with Fourier potentials U_{ij} (which here include the mass ratio $m/m_0 = \gamma$), double wave number $2k$, eigenvalue (*Anpassung*) γ and excitation errors s_g, can be represented by a hyperbola in the s_2, s_3 plane:

$$(2ks_2 - 2k\gamma + U_{12}^2/2k\gamma)(2ks_3 + 2k\gamma + U_{13}^2/2k\gamma) = (U_{23} + U_{12}U_{13}/2k\gamma)^2 \quad (1)$$

in the centrosymmetric case $U_{ij} = U_{ji}$. When the right-hand side is equal to zero, the hyperbola degenerates into two straight lines, which intersect at the point

$$2ks_2 = U_{12}(U_{23}/U_{13} - U_{13}/U_{23})$$
$$2ks_3 = U_{13}(U_{23}/U_{12} - U_{12}/U_{23}), \quad (1a)$$

i.e. the diffraction condition at which the accidental degeneracy occurs. It is noted that this degeneracy may occur only in the centrosymmetric case or, rather, when the phase invariant $\alpha_2 - \alpha_3 - \alpha_{23} = n\pi$, see *e.g.* Marthinson, Matsuhata, Høier & Gjønnes (1988). Experimentally, this condition is observed as vanishing contrast at the position given by (1*a*) on the Kikuchi or Kossel line. In principle, two equations are obtained; in practice, at best one of the excitation errors can be measured with sufficient accuracy.

The above treatment can be extended to four beams. In the eigenvalue equation $AC = 2k\gamma C$, let us write the four-beam matrix

$$A = \begin{bmatrix} 0 & U_{12} & U_{13} & U_{14} \\ U_{21} & 2ks_2 & U_{23} & U_{24} \\ U_{31} & U_{32} & 2ks_3 & U_{34} \\ U_{41} & U_{42} & U_{43} & 2ks_4 \end{bmatrix}.$$

In the general case ($U_{ij} = U_{ij}^*$), the dispersion equation for the eigenvalues γ can be written

$$|A - \gamma I| = XYZ + pX + qY + tZ + C = 0 \quad (2)$$

with

$$X = 2ks_2 + \gamma + (U_{21}U_{12}/\gamma)$$
$$Y = 2ks_3 - \gamma + (U_{31}U_{13}/\gamma)$$
$$Z = 2ks_4 - \gamma + (U_{41}U_{14}/\gamma)$$
$$p = -U_{31}U_{14}[(1/\gamma) + (U_{43}/U_{13}U_{41})]\text{c.c.}$$
$$q = -U_{41}U_{12}[(1/\gamma) + (U_{24}/U_{14}U_{21})]\text{c.c.}$$
$$t = -U_{21}U_{13}[(1/\gamma) + (U_{23}/U_{21}U_{13})]\text{c.c.}$$
$$C = U_{12}U_{21}U_{13}U_{31}U_{14}U_{41}[(1/\gamma) + (U_{43}/U_{13}U_{41})] \times [(1/\gamma) + (U_{24}/U_{14}U_{21})] \times [(1/\gamma) + (U_{23}/U_{21}U_{13})] + \text{c.c.}$$

c.c. represents the complex conjugate. The parameters X, Y, Z, p, q, t and C are all real numbers when A is Hermitian. Equation (2) represents a set of hyperbolic surfaces in the three-dimensional XYZ space. In analogy with the three-beam case, let us look for degenerate points in the centrosymmetric case – and in other cases when $C^2 + 4pqt = 0$ owing to some symmetry element.

Assuming for the moment $Z \neq 0$ in (2), we may write

$$[X + (q/Z)][Y + (p/Z)] = -\{t^{1/2} + [(-pq)^{1/2}/Z]\}^2.$$

When the right-hand side is zero, the hyperbolae at constant Z degenerate into two straight lines intersecting at the point where

$$X = -C/2p, \quad Y = -C/2q, \quad Z = -C/2t. \quad (3)$$

Equations (3) can be regarded as a parametic representation of a curve in XYZ space by the eigenvalue

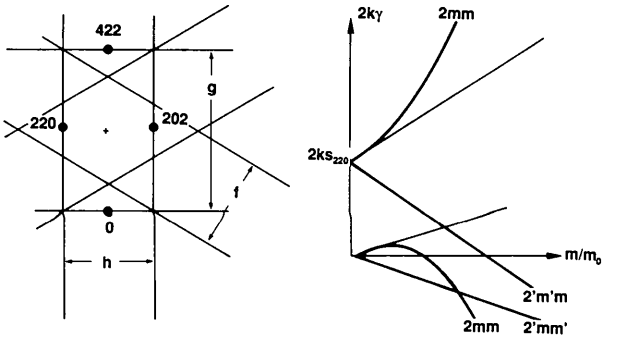

(*a*) (*b*)

Fig. 1. (*a*) Sketch of beams and Kikuchi lines in a four-beam $2mm$ case. The coordinates δ and ε for the wave point are measured from the $2mm$ point. (*b*) Four-beam dispersion surface branches at the symmetric wave point $2mm$, as functions of the mass ratio β. Critical voltage occurs when the branches $2mm$ and $2'mm'$ intersect.

γ. At any voltage, there is a relation between the magnitudes X, Y and Z, *viz* the Ewald sphere; the degeneracy occurs where the curve cuts this sphere. The assumption $Z \neq 0$ is seen to be unnecessary because (3) is also obtained by division by X or Y. Note also that p, q or $t = 0$ can be avoided by redefining the zero beam.

As in the three-beam case, the degeneracies occur only in the centrosymmetric case and other cases where the invariant phase angles are 0 or π because of some symmetry element. Symmetry considerations are, in general, helpful in deriving the condition for degeneracies; the most useful cases seem to appear between Bloch waves of opposite symmetry referred to a symmetry element.

3. Example I: diamond-shaped configuration of spots

As the first example, consider the situation sketched in Fig. 1(*a*): four beams in a configuration with point symmetry 2*mm*. This is essentially the case studied by Gjønnes & Høier (1971) who showed how the 220 structure factor in silicon could be determined from the position of vanishing contrast at the 422 Kikuchi line, *i.e.* at one of the mirror lines; see also Spellward (1988). The effect appears with much clearer contrast in the CBED pattern as shown in Fig. 2. This case was discussed also by Marthinsen, Matsuhata, Høier & Gjønnes (1988); here, we present a treatment of this four-beam case based on the expressions derived above, with a more general proof.

With the Fourier potentials $U_{13} = U_{14} = U_{23} = U_{24} = f$, $U_{34} = U_g$ and $U_{12} = U_h$ and with the excitation errors

$$2ks_3 = (h^2 - g^2)/4 - g\delta + h\varepsilon$$
$$2ks_4 = (h^2 - g^2)/4 + h\varepsilon$$
$$2ks_2 = g\varepsilon$$

(δ and ε are orthogonal coordinates, measured from the symmetry point 2*mm*, *cf.* Fig. 1*a*) inserted in the expressions for X, Y, Z, C, p, q and t, equations (3) take the forms

$$\begin{aligned}
&2h\varepsilon + (U_h^2/\gamma) - \gamma \\
&\quad = U_h^2[(1/\gamma) + (1/U_h)]^2[(1/\gamma) + (U_g/U_f^2)]^{-1} \\
&[(h^2 - g^2)/4] - g\delta + h\varepsilon + (U_f^2/\gamma) + \gamma \\
&\quad = U_f^2[(1/\gamma) + (U_g/U_r^2)] \qquad (4) \\
&[(h^2 - g^2)/4] + g\delta + h\varepsilon + (U_f^2/\gamma) - \gamma \\
&\quad = U_f^2[(1/\gamma) + (U_g/U_f^2)].
\end{aligned}$$

From the last two equations, we obtain $\delta = 0$, $2ks_3 = 2ks_4$ and $\gamma = [(h^2 - g^2)/4] + h\varepsilon$, which, inserted in the first equation, yield two values for ε:

$$\begin{aligned}
h\varepsilon = (\{-[(h^2 - g^2)/4 + (-2U_h^2 + U_g^2 + U_g U_f)/U_g\} \\
\times \{-[(h^2 - g^2)/4] + U_g - U_f\})^{1/2}. \qquad (5)
\end{aligned}$$

For the case where $g > h$, these are the location of two critical points at the mirror line $\delta = 0$, visible as vanishing contrast of the reflection g, with the central beam at beam 3. The corresponding degeneracies occur between a symmetric (m) and an antisymmetric (m') Bloch wave. With increasing voltage, $|\varepsilon|$ will decrease until the two degeneracies merge at a

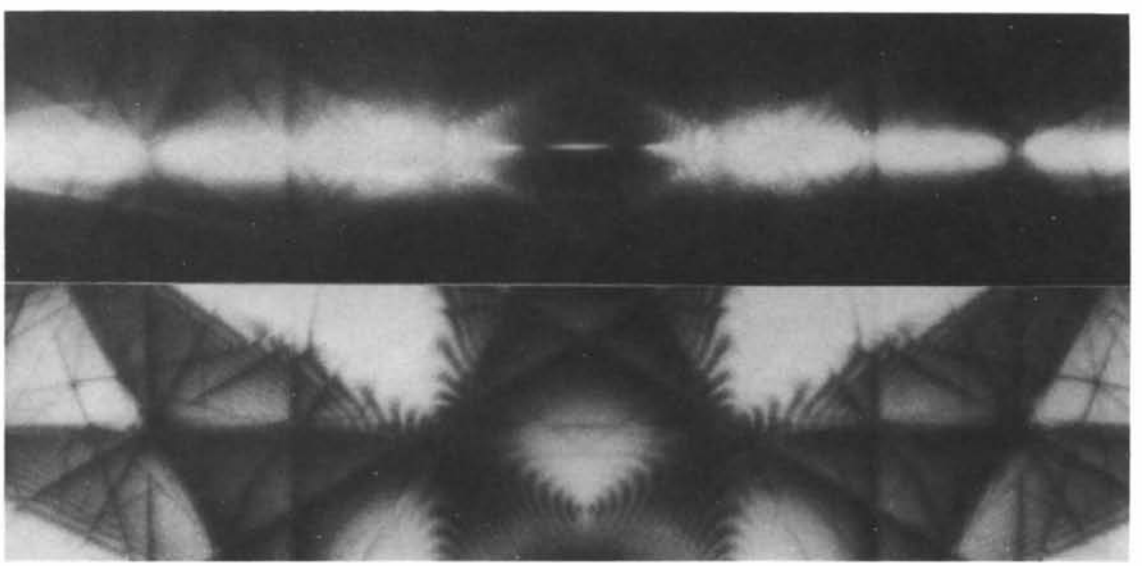

Fig. 2. Large-angle convergent-beam electron diffraction (LACBED) patterns from silicon taken at 203 kV, in 000 and 422 reflection, showing vanishing contrast at two positions on the 422 line.

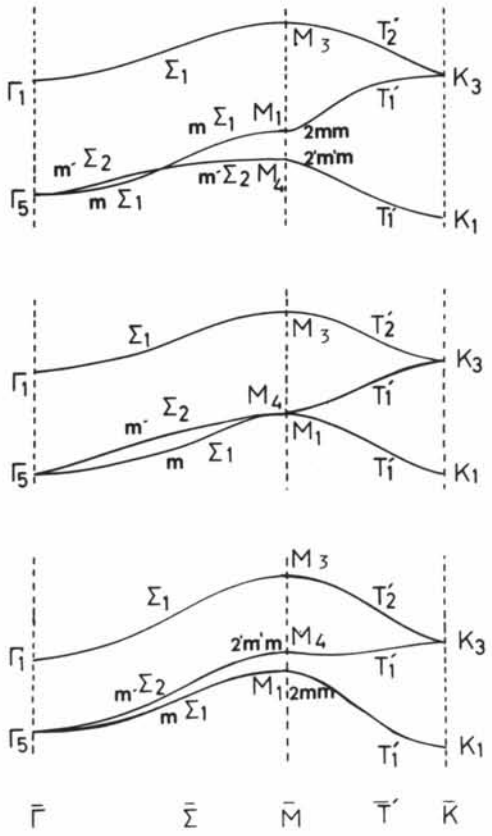

Fig. 3. Calculated dispersion surfaces (from top to bottom) below, near and above the critical voltage along the two symmetry lines in Fig. 1(*a*). Branches are labelled according to both solid-state and crystallographic notations. The calculations are for ZnS with 42 beams.

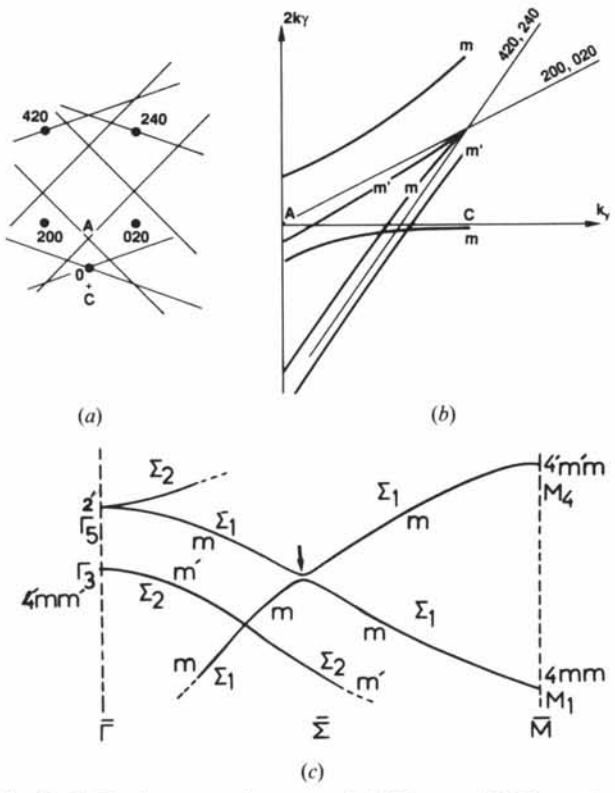

Fig. 4. (*a*) Five-beam case in copper, in [001] zone. (*b*) Schematic five-beam dispersion suface section along k_y, at the critical voltage when the accidental degeneracy appears between two *m* branches. (*c*) 64-beam calculation at 100 kV of the dispersion surface in copper. Bloch waves 4, 5 and 6 are shown at 100 kV; the accidental degeneracy between 4 and 5 is indicated by an arrow.

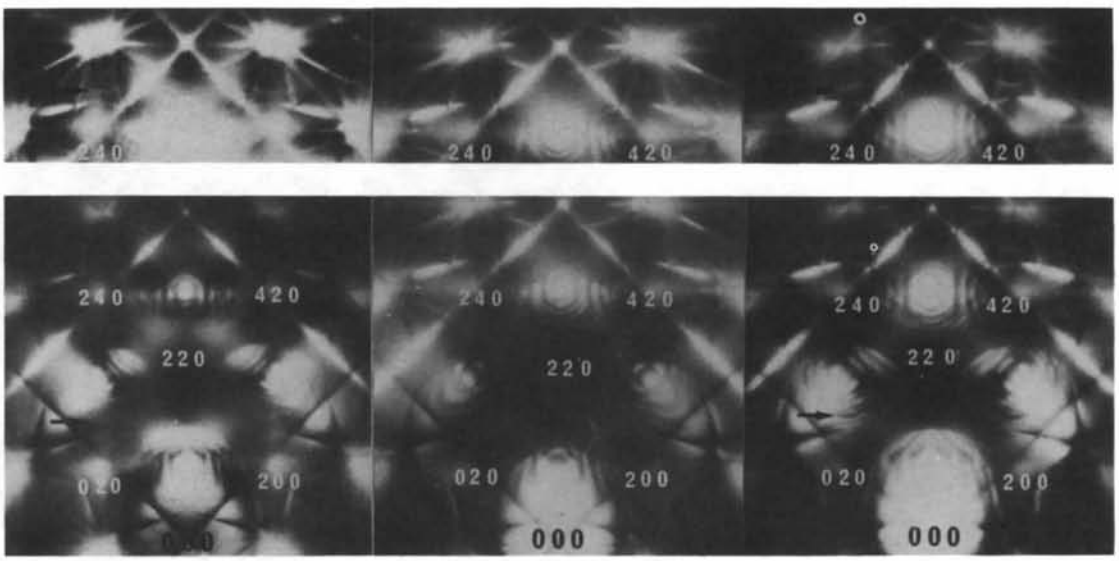

Fig. 5. Left to right: CBED patterns taken from copper at 82, 122 and 203 kV, respectively. The upper correspond to parts of the lower picture with a different exposure time.

Table 1. *Some calculated nonsystematical critical voltages* (kV) *in the 2mm configuration of Fig.* 1(*a*) *for* Ca 100 *beams with Doyle–Turner scattering factors and available Debye–Waller factors*

ZnS	165 obs: 152 (5)
GaAs	129
Germanium	149
Silicon	293
Copper	532
Aluminium	1345

critical voltage, given by

$$E_c = (m_0c^2/e)\{[U_g(g^2 - h^2)/4(2U_f^2 - U_gU_h - U_g^2)] - 1\}$$

in terms of Fourier potentials referred to zero rest mass. Equation (5) for the position of the degeneracies can also be derived by putting the central beam at beam 3 at the outset, noting that $\gamma = U_{34}$ is then a solution, which makes C, p and $t = 0$. Inserting this back into the determinantal equation (2), we obtain $XZ = -q$ as a condition for the degeneracy, with the same result as before.

A further alternative is referred to in Matsuhata & Gjønnes (1988): along the mirror line, the four-beam matrix will have three symmetric and one antisymmetric Bloch-wave solutions. The latter ($C_1 = C_4 = 0$; $C_2 = -C_3$) is readily seen to have the eigenvalue $\gamma = -U_g$; the degeneracy occurs where one of the symmetrical eigenvalues coincides with γ. A schematic dispersion surface is shown in Fig. 1(*b*).

In the f.c.c. 422 case studied, $\beta U_g = \beta U_{422} = U_{34}$; $\beta U_f = \beta U_h = \beta U_{220} = U_{12} = U_{13}$. With positive Fourier potentials, as in the example treated here, the degeneracies will appear at the short diagonal of the diamond formed by beams 1 and 2. In cubic-close-packed diamond and sphalerite structures, this degeneracy is quite easy to observe and measure on the 422 Kikuchi or Kossel line, either as the separation 2ε between the degenerate wave points or as the critical voltage at which they coalesce. Fig. 2 is an example from silicon. In Table 1, some calculated critical voltages for the 422 extinction are listed. Fig. 3 shows an example of many-beam calculations for ZnS: branches 2, 3 and 4 as functions of the separation from the symmetry point M in Fig. 1(*a*), along two directions.

A variation on this symmetrical four-beam case is the 'skew diamond' configuration with symmetry 2. For this case, the four-beam analytical expression at the symmetric point 2 can be found by equating the eigenvalues for one symmetric and one antisymmetric Bloch wave (see Appendix).

4. Example II: extinction in a five-beam case *hk*0 in copper

This case is sketched in Fig. 4(*a*); a schematic dispersion surface for the five most important beams 000, 200, 020, 420 and 240 is shown in Fig. 4(*b*) as a section along the mirror line m in Fig. 4(*b*), with two antisymmetric and three symmetric Bloch waves. Two degeneracies are seen near the Bragg condition for simultaneous excitation of 420 and 240, *i.e.* at the split Kikuchi lines separated through the strong 220

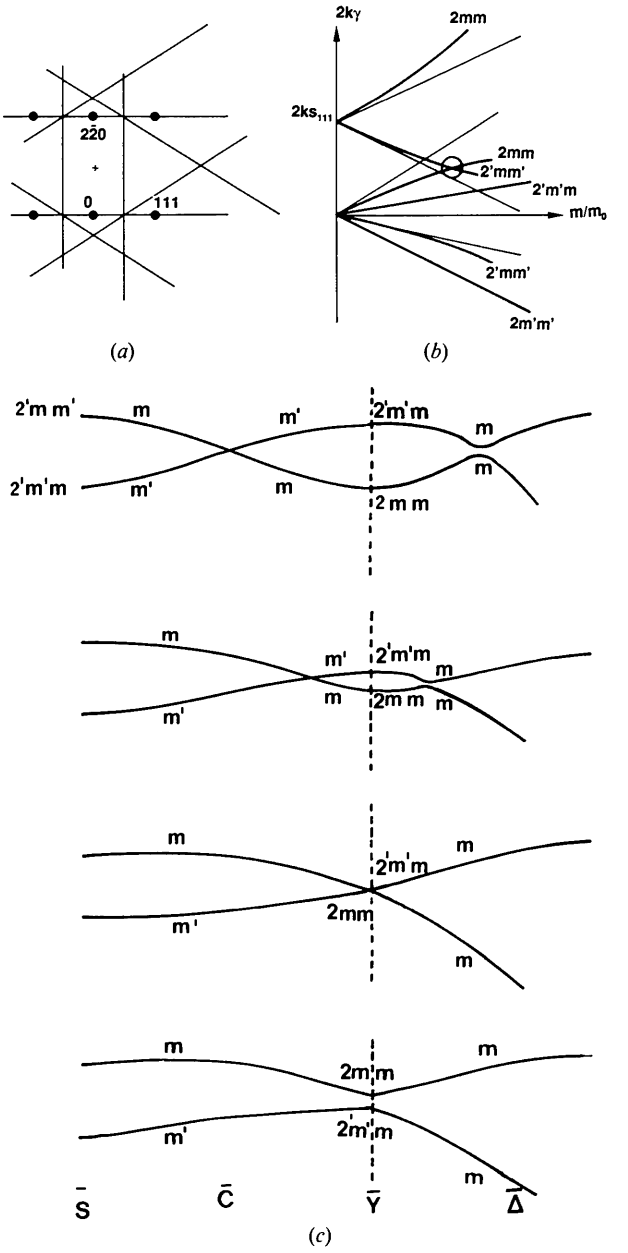

Fig. 6. (*a*) A six-beam case 000, 2$\bar{2}$0, 11$\bar{1}$, $\bar{1}$11, 3$\bar{1}$1, 1$\bar{3}$1 in the 112 projection in MgO. (*b*) Sketch of six branches at the wave point Y as functions of the mass ratio β; a critical voltage is found that corresponds to the intersection between the branches 2 and 3 ($2mm^{(2)}$ and $2'mm'^{(1)}$). (*c*) 96-beam calculations of the branches 2 and 3 around the Y point at voltages 80, 200 and 300 kV, schematic as functions of k_x and k_y [(*a*)]. An accidental degeneracy is seen at the C line.

coupling. One of these, between one symmetric and one antisymmetric branch, will appear at any voltage; the other, between the symmetrical branches 2 and 3, will appear only at a particular primary-beam voltage. This voltage can be deduced from the reduced matrix

$$\begin{bmatrix} -2k\gamma & 2^{1/2}\beta U_{200} & 2^{1/2}\beta U_{420} \\ 2^{1/2}\beta U_{200} & \beta U_{220}+2k(s_1-\gamma) & \beta(U_{220}+U_{400}) \\ 2^{1/2}\beta U_{420} & \beta(U_{220}+U_{400}) & \beta U_{220}+2k(s_2-\gamma) \end{bmatrix}$$

for the symmetrical Bloch waves (see, *e.g.*, Kogiso & Takahasi, 1977). From the standard formulae referred to above for the three-beam degeneracy equation (1*a*), we obtain, for the excitation errors s_1 and s_2 for 200 and 420, respectively,

$$\begin{aligned} 2ks_1/\beta = &-U_{220}+U_{200}\{[(U_{220}+U_{400})/U_{420}] \\ &-[2U_{420}/(U_{220}+U_{400})]\} \\ 2ks_2/\beta = &-U_{220}+U_{420}\{[U_{220}+U_{400}/U_{200}] \\ &-[2U_{200}/(U_{220}+U_{400})]\}, \end{aligned}$$

which must be fulfilled simultaneously. At the mirror line m, there is an additional relation between the two excitation errors, from which we can obtain the voltage for this degeneracy appearing at the line m:

$$\begin{aligned} E_c = (m_0c^2/e)[(g^2/\{[(3U_g^2 - U_m^2)(U_h + U_f)/U_gU_m] \\ - [4U_gU_m/(U_h + U_f)] - 2U_h\}) - 1], \end{aligned}$$

where $U_g = U_{200}$, $U_h = U_{220}$, $U_f = U_{400}$ and $U_m = U_{420}$.

In the patterns in Fig. 5, taken at 82, 102 and 122 kV, respectively, two branches of the split 420, 240 lines are seen at the low and high voltages but with very weak contrast at the intermediate voltage. The 64-beam calculated dispersion surface branches in Fig. 4(*c*) correspond to 100 kV.

5. Example III: a six-beam case in MgO

As a third example, consider the symmetric six-beam configuration of Fig. 6, near the 211 zone axis in MgO, where a critical voltage was found at the Y point. Results of eigenvalue calculations with 86 beams along the mirror lines $C(s_{022} = 0$ and $s_{11\bar{1}} =$

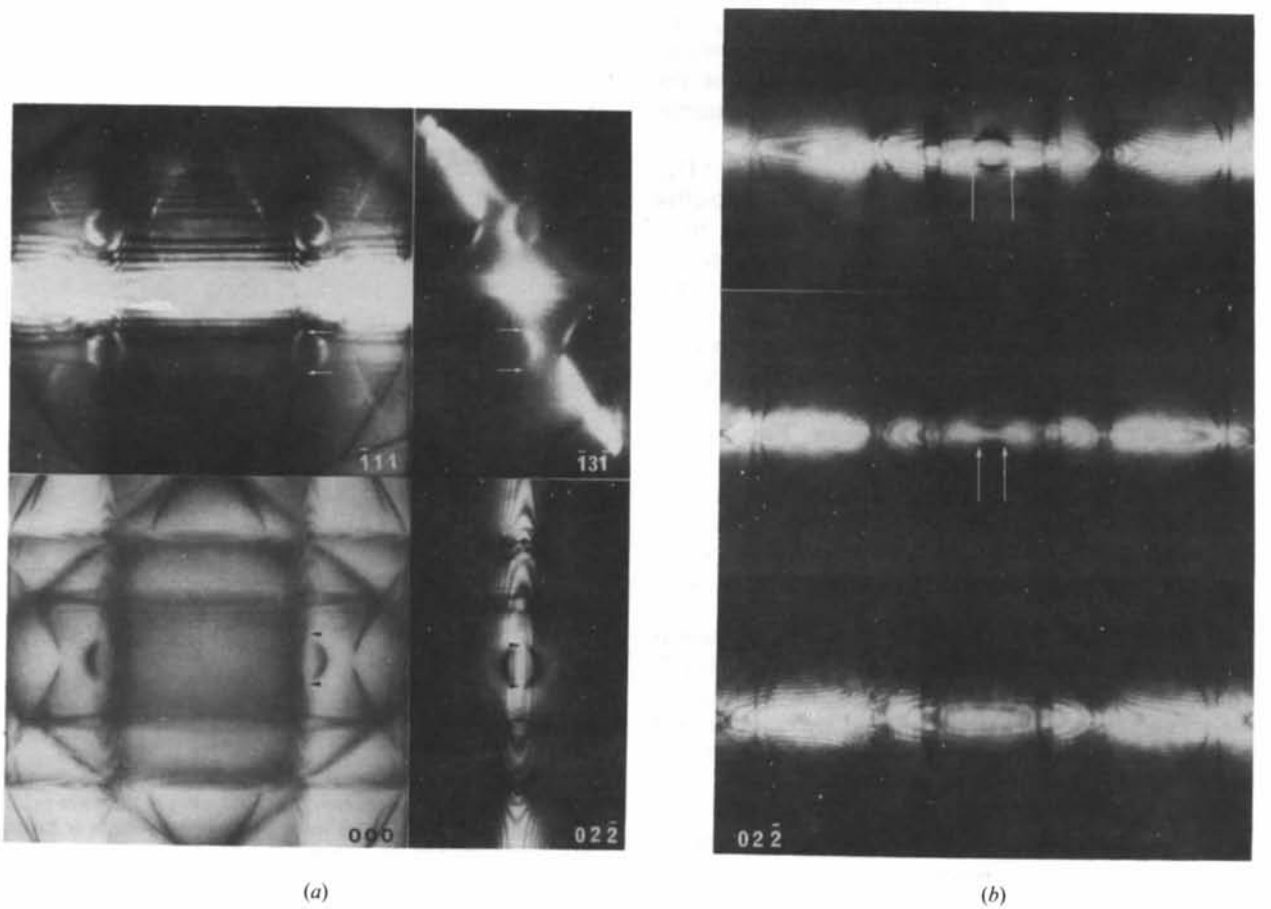

(*a*) (*b*)

Fig. 7. LACBED patterns of MgO at the 211 zone axis. (*a*) Bright-field patterns taken at 163 kV. The position of the accidental degeneracy is indicated by the arrows. (*b*) Dark-field LACBED of 220 taken at 163, 230 (nominal) and 300 kV (nominal).

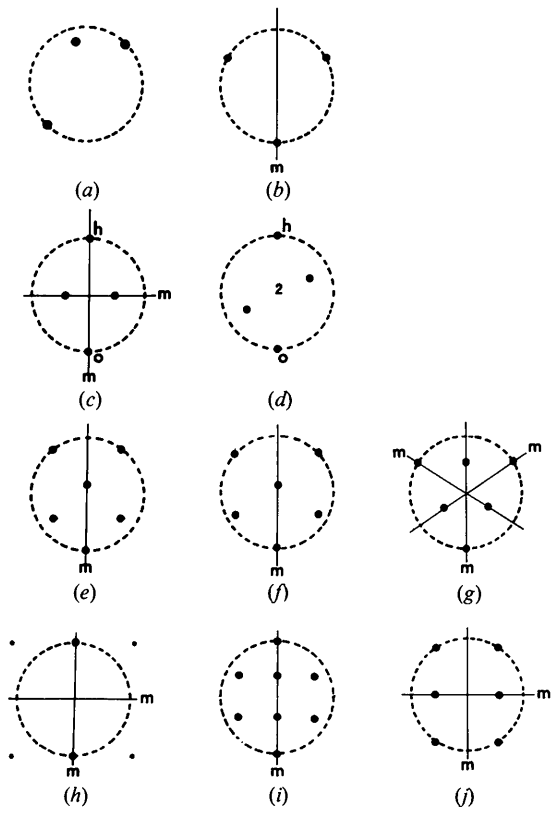

Fig. 8. Diffraction situations with nonsystematic critical voltages; with point symmetries: (*a*) 1 (general triangle); (*b*) *m* (symmetrical triangle); (*c*) 2*mm* – in centred projection, *C*2*mm*; (*d*) 2 ('skew diamond'); (*e*), (*f*), (*g*) *m* (*cf.* §4) in 4*mm*, *C*2*mm* and 6*mm* projections, respectively; (*h*) 2*mm* with superlattice reflections; (*i*) 4*mm*; (*j*) 2*mm* (*cf.* §5).

$s_{\Pi 1}$) are shown in Fig. 6(*b*) for three different voltages. Degeneracies appear at the *C* line; on increasing voltage, they move towards the 2*mm* symmetry point *Y*, where they merge at a critical voltage. An analytical expression for the degenerate eigenvalue can be obtained by equating two solutions from the reduced matrices with 2*mm* and 2′*m*′*m* symmetry, *i.e.*

$$2k\gamma_{2mm} = (1/2)\{2ks_g + 2U_2 + U_5 + U_4 - [(2ks_g + U_5 + U_4)^2 + 8(U_1 + U_3)^2]^{1/2}\}$$

$$2k\gamma_{2'm'm} = (1/2)\{2ks_g - 2U_2 + U_5 - U_4 + [(2ks_g + U_5 - U_4)^2 + 8(U_1 - U_3)^2]^{1/2}\},$$

where $U_1 = \beta U_{111}$, $U_2 = \beta U_{022}$, $U_3 = \beta U_{131}$, $U_4 = \beta U_{240}$, $U_5 = \beta U_{222}$ and $\beta = m/m_0$. These eigenvalues depend to a first approximation on U_{022} and s_g, but through the dynamical interactions the critical voltage is sensitive also to U_{111}. Using scattering factors for neutral atoms (Doyle & Turner, 1968), we obtained the critical voltage at the *Y* point 234 kV, while the experimental U_{111} found by Lehmpfuhl (1972) gave 258 kV. Our experimental value for the nonsystematic critical voltage obtained from the LACBED patterns in Fig. 7 was found to be in the range 260–270 kV.

6. Configurations for nonsystematic critical voltages

In addition to the three cases discussed above, several other configurations will include useful accidental nonsystematical critical voltages. Some of these are sketched in Fig. 8, which we discuss only briefly. Black dots are reflections and the broken

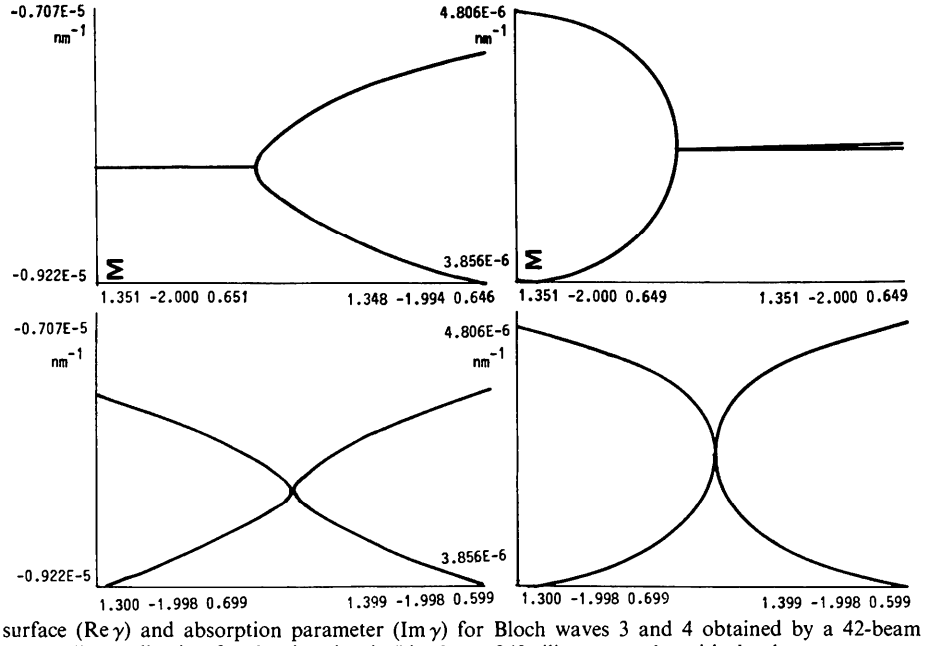

Fig. 9. Dispersion surface (Re γ) and absorption parameter (Im γ) for Bloch waves 3 and 4 obtained by a 42-beam non-Hermitian diagonalization for the situation in Fig. 2, *i.e.* 242 silicon near the critical voltage.

circles indicate the approximate position of the Laue circle. Fig. 8(*a*) shows the general three-beam case discussed by Gjønnes & Høier (1971) [see (1)]. The symmetric three-beam configuration in Fig. 8(*b*) may be seen as a special case of that of Fig. 8(*a*), with the degeneracy appearing on the mirror line at any voltage (Taftø & Gjønnes, 1985), essentially an intersecting-Kikuchi-line situation. Fig. 8(*c*) is the diamond-shaped array of spots in a *Cmm* projection, discussed in §3 above. This can also be used in a *pmg* projection; then, the degeneracy will appear outside the Laue circle. A skew variant of this is shown in Fig. 8(*d*), with critical voltage at the symmetry point 2 (see Appendix) Figs. 8(*e*) and (*f*) are variations on the case of Fig. 8(*c*) above, near axes 4*mm* and 2*mm*, respectively, with Fig. 8(*g*) showing a further variation expected in a centred projection. Fig. 8(*h*) is then case III above (§5); with Fig. 8(*i*) as an extension of the third-order critical voltage of Hewat & Humphreys (1975), essentially the same as Fig. 8(*h*), or as an extension of the second-order systematical critical voltage. The sensitivity varies considerably among these. So far the diamond and skew diamond configurations of Figs. 8(*c*) and (*d*) appear to be the best. Higher sensitivity is expected when the intersecting branches meet at a shallow angle, so there is lower sensitivity with higher-order reflections. Some degeneracies, as in Fig. 8(*b*), may not be called critical voltages because the measurement will focus on position rather than acceleration voltage. In general, the measurements are best performed in symmetric configurations, in which case the condition of centrosymmetry is less strict.

Absorption effects are not included in the above treatment. Absorption may shift the degeneracy off the symmetry line or point and also change the critical voltage slightly. This conclusion emerged from calculations based on non-Hermitian diagonalization. An example is shown in Fig. 9 for the silicon 422 case shown in Fig. 2. The two sections, along the *K* line and normal to it, show the degeneracy to prevail but to be slightly shifted off the line. A notable feature is the dispersion-surface shape, which is reminiscent of the reflection case. The effect on the critical voltage was found to be negligible.

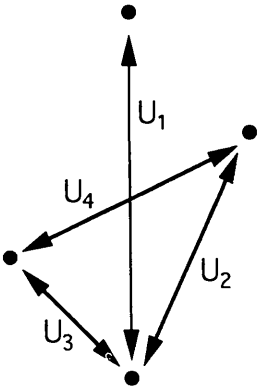

Fig. 10 Configuration of reciprocal-lattice points for the case in the Appendix.

7. Concluding remarks

The nonsystematic critical voltage can be found in a number of configurations and measured with an accuracy approaching the systematical case. Analytical solutions referred to in this paper, together with symmetry reduction of the dispersion matrix of the type discussed by Fukuhara (1966) and Kogiso & Takahashi (1977), for example, may be sufficient to estimate the existence and range of useful Bloch-wave degeneracies in the nonsystematic cases. Accurate calculations may need many beams; absorption appears to have a negligible effect on the condition for the degeneracy but may have considerable influence on the intensity distribution in the vicinity of the point of vanishing contrast.

Financial support from the Royal Norwegian Research Council for Scientific and Industrial Research and from the Norwegian Research Council for Science and the Humanities is gratefully acknowledged.

APPENDIX

To a four-beam case with symmetry 2 ('skew diamond') (Fig. 10) correspond two symmetric (2) and two antisymmetric (2′) Bloch waves:

$$\gamma^{1,3} = [(2ks + U_4 + U_1)/2] \pm \{[(2ks + U_4 - U_1)^2/4] + (U_2 + U_3)^2\}^{1/2}$$

$$\gamma^{2,4} = [(2ks - U_4 - U_1)/2] \pm \{[(2ks - U_4 - U_1)^2/4] + (U_2 - U_3)^2\}^{1/2}.$$

References

COCHRAN, W. (1952). *Acta Cryst.* **5**, 630–633.
DOYLE, P. A. & TURNER, P. (1968). *Acta Cryst.* A**24**, 390–397.
FUKUHARA, A. (1966). *J. Phys. Soc. Jpn*, **21**, 2645–2662.
GEVERS, R., SERNEELS, R. & DAVID, M. (1974). *Phys. Status Solidi B*, **66**, 471–482.
GJØNNES, J. & HØIER, R. (1971). *Acta Cryst.* A**27**, 313–316.
GJØNNES, J. & TAFTØ, J. (1978). *Electron Diffraction* 1927–1977, edited by P. J. DOBSON & C. J. HUMPHREYS, pp. 150–155. *Inst. Phys. Conf. Ser.* No. 43. Bristol: Institute of Physics.
HEWAT, E. & HUMPHREYS, C. J. (1975). *High-Voltage Electron Microscopy*, edited by P. R. SWANN, pp. 52–56. London: Academic Press.
HURLEY, A. C. & MOODIE, A. F. (1980). *Acta Cryst.* A**36**, 737–738.
KAMBE, K. (1957). *J. Phys. Soc. Jpn*, **12**, 13–36.

KOGISO, M. & TAKAHASHI, H. (1977). *J. Phys. Soc. Jpn*, **42**, 223–229.
LEHMPFUHL, G. (1972). *Z. Naturforsch. Teil A*, **27**, 425–433.
MARTHINSEN, K., MATSUHATA, H., HØIER, R. & GJØNNES, J. (1988). *Aust. J. Phys.* **41**, 449–459.
MATSUHATA, H. & GJØNNES, J. (1988). *Proc. EUREM* 88, *Inst. Phys. Conf. Ser.* No. 93, Vol. 2, pp. 19–20.
MATSUHATA, H. & STEEDS, J. W. (1987). *Philos. Mag.* **B55**, 17–38.
NIEHRS, H. & WAGNER, E. H. (1955). *Z. Phys.* **143**, 285–299.
REIMER, L. (1989). *Transmission Electron Microscopy*, 2nd ed., p. 286. Berlin: Springer.
SELLAR, J. R., IMESON, D. & HUMPHREYS, C. J. (1980). *Acta Cryst.* A**36**, 686–696.
SHANNON, M. D. & STEEDS, J. W. (1977). *Philos. Mag.* A**36**, 307.
SPELLWARD, P. (1988). *Proc. EUREM* 88, *Inst. Phys. Conf. Ser.* No. 93, Vol. 2, pp. 31–32.
TABBERNOR, M. A., FOX, A. G. & FISHER, R. M. (1990). *Acta Cryst.* A**46**, 165–170.
TAFTØ, J. & GJØNNES, J. (1985). *Ultramicroscopy*. **17**, 329–334.
WATANABE, D., UYEDA, R. & FUKUHARA, A. (1969). *Acta Cryst.* A**25**, 138–140.

Acta Cryst. (1994). A**50**, 115–123

A Study of the Structure Factors in Rutile-Type SnO_2 by High-Energy Electron Diffraction

BY H. MATSUHATA,* J. GJØNNES AND J. TAFTØ

Department of Physics, University of Oslo, PO Box 1048 *Blindern*, 0316 *Oslo, Norway*

(*Received* 29 *March* 1993; *accepted* 12 *July* 1993)

Abstract

The structure factors for low-order reflections of rutile-type SnO_2 have been studied by high-energy electron diffraction. A systematic critical-voltage effect on 220 in 110 systematic reflections, a nonsystematic critical-voltage effect on $1\bar{5}0$ at the [513] zone axis, a nonsystematic critical-voltage effect on the 002 reflection at the [100] zone axis and a [113]-zone-axis critical-voltage effect were observed within the accelerating-voltage range of a 200 kV electron microscope. Analysis of these critical-voltage effects gave experimental values for the structure factors between the theoretical values obtained for the $Sn^{2+}O_2^{1-}$ and $Sn^{4+}O_2^{2-}$ states for low-order reflections like 110 and 011, whereas a structure-factor value between the theoretical values for the neutral SnO_2 and $Sn^{2+}O_2^{1-}$ states was found for the 121 reflection.

1. Introduction

The rearrangement of outer electrons in atoms owing to the bonding in a crystal can be studied by diffraction experiments, in particular at low values of the scattering variable. In this range, electron diffraction will be more sensitive than X-ray diffraction to changes in the atomic scattering factors f^x, as seen from the Mott relation:

$$f^{el}(s) = (me^2/2h^2)[Z - f^x(s)]/s^2,$$

where $s = \sin\theta/\lambda$ and θ, λ, Z, $f^{el}(s)$ and $f^x(s)$ are the scattering angle, electron wavelength, atomic number, electron scattering factors and X-ray scattering factors, respectively; see, for example, Hirsch, Howie, Nicholson, Pashley & Whelan (1965). This advantage is exploited in several electron diffraction methods. Measurement and analysis of the critical-voltage effect (Watanabe, Uyeda & Fukuhara, 1969) caused by the accidental degeneracy of the Bloch wave offer accurate and absolute measurements related to structure factors for low-order reflections, thus providing information on the distribution of outer electrons. Until recently, the critical-voltage effect in the systematic case has been the one mainly utilized. In this case, a high-voltage electron microscope is usually required for the measurement of one or two critical voltages. An extension of the method so that more data for low-order reflections can be obtained and electron microscopes in a more commonly available voltage range can be used appears desirable.

The critical-voltage effect occurs not only in the case of systematic reflections but also in two-dimensional configurations of reflections. Gjønnes & Høier (1971) proposed to extend the method to the nonsystematic case by measuring precise diffraction conditions for the accidental Bloch-wave degeneracy in the Kikuchi pattern. In the preceding paper (Matshuata & Gjønnes, 1994), we presented a development of the nonsystematic critical-voltage method that is applicable in the voltage range of ordinary electron microscopes and that uses the modern convergent-beam technique. Another approach, by

* Present address: Division of Electrodevices, Electrotechnical Laboratory, 1-1-4 Umezono, Tsukuba, Japan.